


Optimizing controlled laser cutting of hard tissue (bone)

Journal Article

Author(s):

Bernal, Lina M. Beltran; Schmidt, Iris T.; Vulin, Nikola; Widmer, Jonas; [Snedeker, Jess Gerrit](#) ; Cattin, Philippe C.; Zam, Azhar; Rauter, Georg

Publication date:

2018-12

Permanent link:

<https://doi.org/https://doi.org/10.3929/ethz-b-000310185>

Rights / license:

[In Copyright - Non-Commercial Use Permitted](#)

Originally published in:

at - Automatisierungstechnik 66(12), <https://doi.org/10.1515/auto-2018-0072>

Applications

Lina M. Beltran Bernal, Iris T. Schmidt, Nikola Vulin, Jonas Widmer, Jess G. Snedeker, Philippe C. Cattin, Azhar Zam and Georg Rauter*

Optimizing controlled laser cutting of hard tissue (bone)

Optimierung von Kontrollierter Laserosteotomie

<https://doi.org/10.1515/auto-2018-0072>

Received May 17, 2018; accepted August 14, 2018

Abstract: Conventional bone surgery leads to unwanted damage to the surrounding tissues and a slow healing process for the patients. Additionally, physicians are not able to perform free cutting shapes due to the limitations of available systems. These issues can be overcome by robot-assisted contactless laser surgery since it provides less mechanical stress, allows precise functional cuts, and leads to faster healing. The remaining drawback of laser surgery is the low ablation rate that is not yet competitive with conventional mechanical piezo-osteotomes. Therefore, we aim at maximizing the efficiency in hard tissue laser ablation by optimizing the lateral movement speed for different irrigation conditions.

The results of this study show a non-linear relationship between cutting rates, speeds, and depths that should be critically considered for integration in robotic laser surgery.

Keywords: laser osteotomy, cutting bone, automation, laser, irrigation, cutting velocity

Article note: Lina M. Beltran Bernal and Iris T. Schmidt contributed equally to this paper.

***Corresponding author: Georg Rauter**, BIROMED-Lab, Department of Biomedical Engineering, University of Basel, Allschwil and Sensory-Motor Systems Lab, ETH Zurich and Spinal Cord Injury Center, University Hospital Balgrist, Zurich, Switzerland, e-mail: georg.rauter@unibas.ch

Lina M. Beltran Bernal, Iris T. Schmidt, Azhar Zam, BLOG, Department of Biomedical Engineering, University of Basel, Allschwil, Switzerland, e-mails: lina.beltran@unibas.ch, iris.schmidt@unibas.ch, azhar.zam@unibas.ch

Nikola Vulin, Jonas Widmer, Jess G. Snedeker, Department of Orthopaedics, University of Zurich, Institute for Biomechanics, ETH Zurich, Zurich, Switzerland, e-mails: nvulin@student.ethz.ch, jonas.widmer@hest.ethz.ch, jess.snedeker@hest.ethz.ch

Philippe C. Cattin, CIAN, Department of Biomedical Engineering, University of Basel, Allschwil, Switzerland, e-mail: philippe.cattin@unibas.ch

Zusammenfassung: Konventionelle chirurgische Eingriffe am Knochen führen zu ungewollten Schäden im umliegenden Gewebe. Außerdem ziehen diese Eingriffe am Knochen einen langsamen Heilungsprozess für den Patienten nach sich. Auch erlauben es herkömmliche chirurgische Systeme den Ärzten nicht freie Schnittformen zu erzielen. Mit robotergestützter kontaktfreier Laserchirurgie können diese Limitierungen jedoch überwunden werden; Laserchirurgie führt zu geringeren mechanischen Spannungen im Gewebe, erlaubt präzise funktionelle Schnitte und lässt den Knochen schneller heilen. Bleibt allein, dass die Schnittgeschwindigkeit in der Laserchirurgie (Laserosteotomie) bis jetzt nicht mit jener von konventionellen Piezoosteotomen mithalten kann. Aus diesem Grund arbeiten wir daran die Effizienz von Laserosteotomie zu erhöhen indem die laterale Laserbewegung für verschiedene Befeuchtungsparameter optimiert wird.

Die Resultate der vorliegenden Studie zeigen ein nicht-lineares Verhältnis von Schnittraten, lateraler Laserbewegung und Schnitttiefe. Diese Erkenntnisse sollten unbedingt berücksichtigt werden, wenn Laserchirurgie in robotergestützten Chirurgiesystemen eingesetzt wird.

Schlagwörter: Laserosteotomie, Knochenschneiden mit Laser, Automatisierung, Laserparameter, Wasserparameter, Schnittgeschwindigkeit

1 Introduction

Laser ablation is an accurate, contactless method for cutting hard tissue in the body. It has been shown that laser osteotomy reduces the healing time of the remaining bone compared to conventional bone cutting with piezoosteotomes. The reason for accelerated healing is that the spongy structure remains intact [1]. Until today, highest ablation rates could be reached using mid-IR laser pulses, such as the erbium-doped yttrium aluminum garnet (Er:YAG) laser, with a wavelength of 2.94 μm . Hereby,

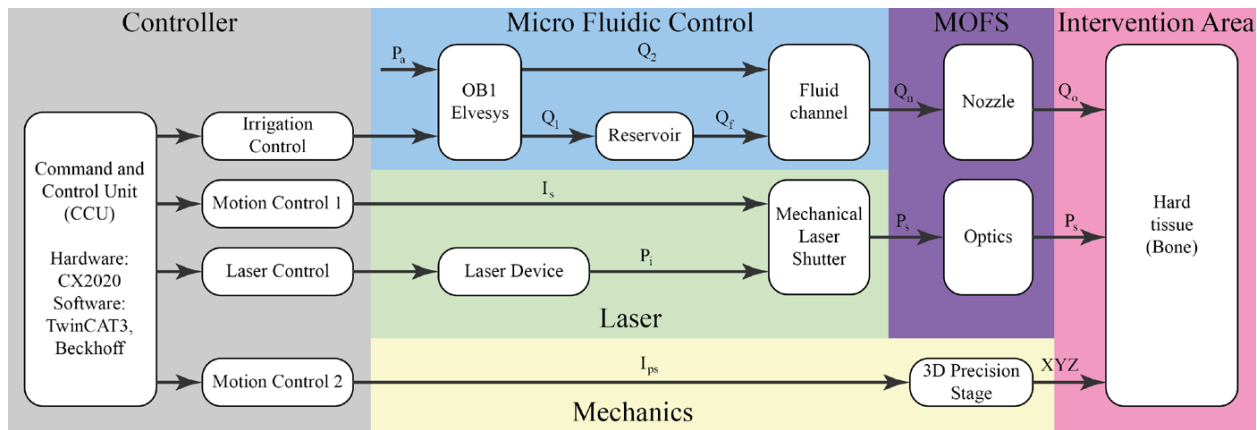


Figure 1: Scheme of the test setup for investigating relative motion between bone and laser on osteotomy performance.

the underlying physical principle of laser ablation is based on thermo-mechanical effects produced by the interaction between the microsecond pulses of the Er:YAG laser working close to one of the highest absorption peaks of water (around $3\ \mu\text{m}$). Namely, ablation is performed by the rapid evaporation of the water content in hard tissue due to the heat transfer from the microsecond laser to the area of interaction, and consequently the clean removal of the target tissue without significant heat transfer to the surrounding bone [2]. Thermo-mechanical ablation, however, reduces the water content of the bone and in order to rehydrate the tissue and consequently prevent carbonization, the lased area has to be irrigated with water [3]. The standard solution for this problem is continuous spraying of the cutting area with water spray [4]. However, since continuous spraying will not only irrigate the bone, but create a layer of water on its surface, the Er:YAG laser cannot be expected to ablate bone efficiently. Thus, a continuous spray will act as a protection against ablation.

To overcome the limitations of laser ablation efficiency in bone due to continuous spraying, we investigated the effect of different discontinuous/pulsed irrigation conditions on ablation efficiency in a previous study [5]. The focus of this paper is to optimize controlled laser cutting of hard tissue (bone) by varying lateral cutting speeds for different irrigation conditions while the laser parameters remain untouched.

To enable controlled optimized laser ablation for minimal invasive surgery, we are developing an automated closed-loop controlled robotic endoscope for laser ablation of bone (laser osteotome) with a microfluidic system for irrigation. In the current development state, the laser is not yet integrated in the robotic endoscope [6, 7, 8, 9] and therefore experiments are carried out in our optics and laser lab [10, 11, 5]. To investigate the influence of different

velocities on the cutting performance, we have developed a test setup mounted on an optical table. This setup allows creating controlled conditions for irrigation, laser, and relative motion between laser and bone (Figure 1). From research of other groups in the field, it is already known that coordinated alternating provision of laser light and irrigation increases the ablation efficiency while carbonization of the hard tissue could be prevented [12]. However, the long waiting time in between the pulses (repetition rate was 0.2 Hz) was not suitable for a real intervention. Moreover, the cutting conditions might change as soon as the laser moves across the bone to create not only single holes in the bone, but also cutting lines. The necessity of optimized parameter settings for laser and irrigation can even be used in an inverted way. Instead of increasing the ablation efficiency, also a desired reduction of the ablation rate can be desirable when the laser cuts get close to delicate tissue such as nerves [13]. However, in this paper, we intend to optimize the lateral cutting speeds for different irrigation settings [5] in order to maximize the ablation efficiency without carbonization of the tissue. We also want to ensure that the ablation has high quality, which means that the bottom of the ablation crater along the lateral cutting direction is smooth and does not consist of single holes leading to perforation rather than continuous cuts.

The achieved cutting depth was measured with an optical coherence tomography (OCT) system, which additionally allowed a visualization of the top and cross-section views of the obtained laser cuts. Using OCT for the evaluation of the ablation crater after performing laser ablation in bone is a very promising approach, since OCT systems can acquire 3-dimensional scans of the light that is reflected and scattered at the bone surface. Typically, these

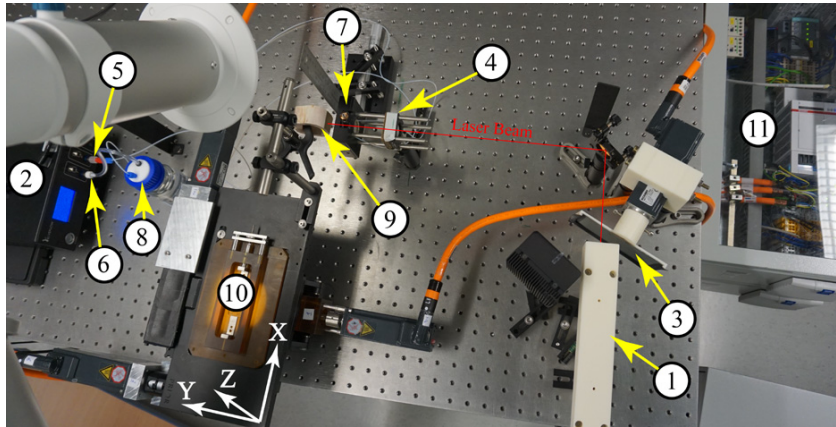


Figure 2: Experimental setup for the laser osteotome.

3-dimensional volumes are in the size of a few millimeters and have a resolution of a few micrometers. That is why, OCT was already used in different studies for measuring laser ablation craters in bone [14, 15, 13, 16]. The non-invasive character of an OCT measurement as well as the possibility to measure the ablated surface in situ and in real-time, makes OCT a smart and promising feedback technique in laser ablation-based osteotomy as other applications in surgery show [17].

2 Methods

Our laser osteotome consists of an Er:YAG laser system (LITETOUCH by Syneron) working at a wavelength of $2.94 \mu\text{m}$, a laser spot diameter of 0.5 mm a repetition rate of 10 Hz , an energy per pulse of 940 mJ , and a pulse duration of $400 \mu\text{s}$. The laser is controlled by a mechanical shutter operated by an AM8111 motor in TwinCAT3 (Beckhoff Automation AG, Germany) at an update rate of 1 kHz . Similarly, a precision stage for microscopes (Prior Scientific, Germany) was equipped with two AM8111 for actuating the bone in the horizontal plane (X and Y-direction). The absolute position resolution of all motors was set to $20 \frac{\text{bit}}{\text{revolution}} \frac{\text{m}}{\text{revolution}}$ and the stages had a spindle steepness of $0.002 \frac{\text{m}}{\text{revolution}}$. For actuation of the Z-direction (vertical axis), a lifting table with scissor kinematics was used (L490/M Thorlabs GmbH, Germany) in combination with another AM8111. A bovine femur bone was rigidly connected with a holder to the XYZ-actuation mechanism. For controlled irrigation, a microfluidic control system, OB1 (Elvesys, France) with two channels was installed; a liquid channel and an air-flow channel that can be controlled individually. The air-flow, Q_2 and water flow Q_f are guided to the focal spot of the laser on the bone surface. Hereby, the air jet can deflect the water jet to allow laser ablation under dry conditions

when the laser pulse is present, and irrigation through a jet of deionized water, when the laser is off (Figure 1).

The experimental setup (Figure 2) operates in the following way: A command computer controls the Er:YAG laser (1) and the pressure source (2). The laser beam is switched on/off by the mechanical shutter (3) and shaped by the optical components (4). The pressure source (2) regulates two airflows, (5) and (6). (5) is guided directly to a nozzle (7). The airflow of (6) is guided into a water reservoir (8) where it is converted into a water flow. The laser, water jet, and air jet are dispensed from the nozzle (7) and focus on the bovine femur bone (9). During the stationary operation of the laser (1) and the pulsed irrigation system (2,5,6,7), the bone can be moved in X-direction at a constant speed with the 3D precision stage (10). After each linear movement in X-direction, the bone can be lowered in Z-position to start a new laser line with a different condition, e. g., different speed in X-direction. In total, the automation system (TwinCAT3, Beckhoff Automation AG, Germany) (11) is set up to realize five different lateral speeds (velocities in X-direction): $v_1 = 0.5 \frac{\text{mm}}{\text{s}}$, $v_2 = 1 \frac{\text{mm}}{\text{s}}$, $v_3 = 2 \frac{\text{mm}}{\text{s}}$, $v_4 = 4 \frac{\text{mm}}{\text{s}}$, $v_5 = 8 \frac{\text{mm}}{\text{s}}$. Higher lateral speeds were not of interest in this study, since the laser would start creating single holes only instead of a continuous line. Also, high tool speeds should be avoided in minimal invasive surgeries for safety reasons, e. g., to allow enough reaction time for the surgeon to stop a process.

Based on this experimental setup of laser, XYZ-stage, and irrigation, we performed two different experiments. The goal was to find the optimal lateral speed that results in the highest ablation efficiency for different irrigation settings and a constant set of laser parameters for single and repeated cuts. Therefore, the first experiment was intended to select the best irrigation conditions out of the two best ones from a previous experiment, where single hole cutting was performed [5]. In the second experiment,

single and repeated cuts were performed at different lateral speeds at fixed irrigation settings to investigate the effectiveness of laser ablation also in deeper cuts.

2.1 Experiment 1

In the first experiment, the bone was actuated at 5 different lateral speeds in X-direction, and therefore, line shapes were ablated. Moreover, we used 2 different irrigation settings that summed up to a total of 10 line cuts. The following irrigation settings were employed:

Table 1: Table of irrigation conditions. Sequences used for the pulsed water jet used in experiment 1. For irrigation condition 1, the duration of one irrigation period was 0.9 s and 1.15 s for irrigation condition 2.

Experiment 1	Water ON duration	Water OFF duration	Water pulse speed	Water volume per pulse
Irrigation condition 1	0.15 s	0.75 s	$1 \frac{\text{m}}{\text{s}}$	$30.4 \mu\text{l}$
Irrigation condition 2	0.25 s	0.9 s	$1 \frac{\text{m}}{\text{s}}$	$50.7 \mu\text{l}$

These irrigation conditions were chosen based on the water jet conditions used in a previous study [5], in which a bovine bone was ablated only in Y-direction, creating single holes. In that study, several irrigation configurations were evaluated in terms of ablated depth and ablated volume in time. Back then when only ablating a hole, the irrigation conditions 1 and 2 provided an ablation rate (ablated bone in depth over time) of $0.37 \frac{\text{mm}}{\text{s}}$ and $0.4 \frac{\text{mm}}{\text{s}}$, respectively.

2.2 Experiment 2

Based on the results of the first experiment, we chose the irrigation condition that led to highest ablation rates overall: irrigation condition 2. The irrigation settings were then kept the same throughout the entire second experiment. Consequently, line cuts were performed with the same 5 different lateral speeds in X-direction as in the first experiment. In particular, we were interested to understand how the lateral cutting velocities impact cutting efficiency for deeper cuts. To do so, the laser moved over the same lines in a repeated way (1 to 5 times). Additionally, the experiment was performed for all five velocity conditions (v_1 to v_5). Thus, the experiment led to a total of 25 different line cuts in 25 Z-positions.

2.3 Setup for measurement of cutting performance

The cross-sections of the line cut profiles were obtained with a custom-made OCT system, based on an Axsun swept laser source ($\lambda_0 = 1060 \text{ nm}$, $\Delta\lambda = 100 \text{ nm}$, sweep rate 100 kHz). The system enables acquiring volumes with a size of up to $7.5 \times 1.6 \times 7.5 \text{ mm}^3$ at a volume rate of $0.37 \frac{\text{volumes}}{\text{s}}$ and preview them at the monitor in real-time. This system has an axial and a lateral resolution of $12 \mu\text{m}$. A general description of these parameters can be found in [18].

For analyzing the depth of each line cut, we acquired OCT B-scans with an extent of 1.6 mm in depth and 2.2 mm lateral extension at the middle of each line cut and perpendicular to the cutting direction (see Figure 3 and Figure 7).

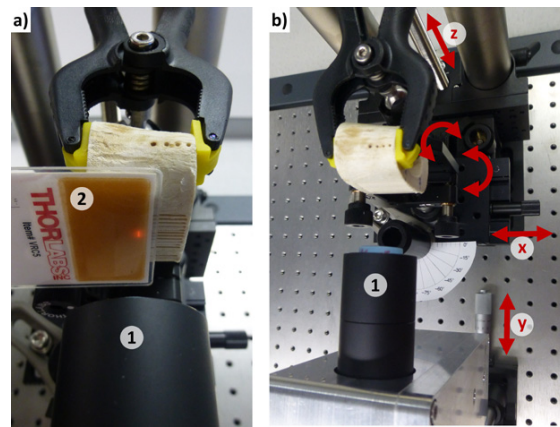


Figure 3: OCT setup: (a) and (b) show how the OCT measurements of the line cuts were set up. The last lens of OCT system (1) focused the beam on the bone surface and scanned a line on the surface. The IR detection card (2) visualized the line scan of the OCT beam (a). The alignment of the bone sample in the focus plane of the OCT system was achieved by using three translation stages (X,Y,Z) and one kinematic mount as indicated with arrows (b).

2.4 Depth measurement

The measurement of the ablation depths of the OCT scans was performed in manual segmentation using ImageJ (see Figure 4). The distance between the deepest point of the cut and the surface of the bone was measured (blue vertical line in Figure 4). We assumed a flat initial bone surface that was the linear connecting surface of the surrounding non-ablated bone regions (yellow horizontal line in Figure 4).

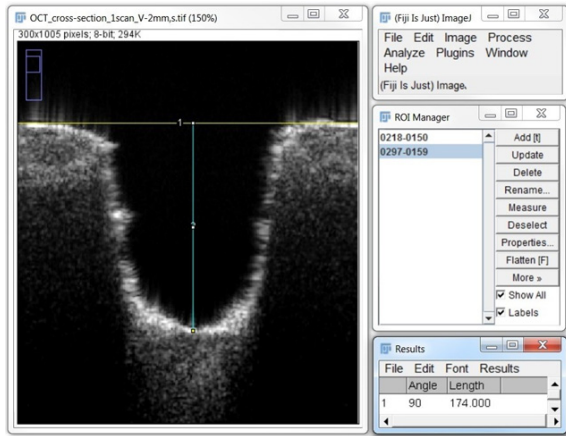


Figure 4: The OCT interface shows an example of the manual depth measurement using ImageJ. In this example, the cutting depth (indicated by the blue vertical line) was measured to be 174 pixels in length that equals to $252 \mu\text{m}$.

3 Results

3.1 Experiment 1

The study in [5] evaluated different water jet cooling conditions for ablating bone by creating single holes. In our study, we used two of those conditions in experiment 1 to create continuous ablations of straight lines. The influence of these two irrigation conditions are evaluated by measuring the ablated depth for the velocities v_1 to v_5 . Figure 5 shows a photograph of the laser cuts for the five different velocities and Figure 6 shows the OCT cross-section and top view images of those ablated areas.

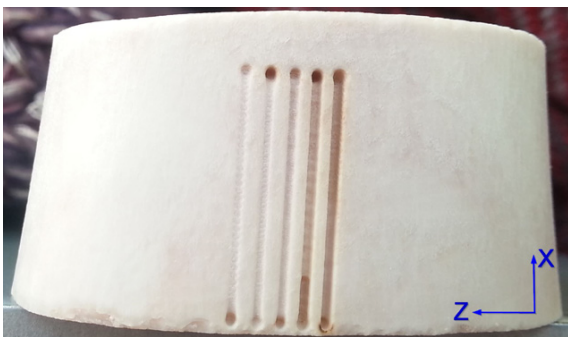


Figure 5: Picture of the resulting laser cuts at 5 different lateral speeds between laser and bone in experiment 1. Each cut line in Z-direction was generated with another constant speed in X-direction (decreasing velocities from left to right). In experiment 2 (not visualized here), new cutting lines were made for the different cutting iterations (1 to 5) at different velocities (v_1 to v_5), therefore, 25 cuts were made in total.

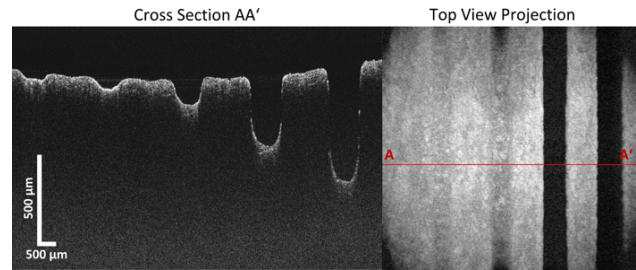


Figure 6: OCT images of the five laser cuts from Figure 5 with different lateral movement speeds (decreasing speed from left to right). Cross section (left image) and top view (right image).

In Table 2, the achieved ablated depths are summarized for the two irrigation conditions and the five speed conditions. The ratios between the ablated depths provide the relative influence of the irrigation conditions on the ablation process. This ratio was calculated by dividing the depth of irrigation condition 2 at a respective velocity (D_2) by the corresponding depth value of the irrigation condition 1 (D_1). The ratio reports the advantage of ablation depth for irrigation condition 2 for values larger than 1 (and vice versa for values smaller than 1). This ratio was calculated for each lateral speed, as well as an overall performance (average of the depth ratio).

Table 2: Table for comparison of irrigation conditions.

Velocity condition [$\frac{\text{mm}}{\text{s}}$]	Cutting depth irrigation condition 1 [μm]	Cutting depth irrigation condition 2 [μm]	Depth ratio [1]
$v_1 = 0.5$	640	637	0.99
$v_2 = 1$	388	372	0.96
$v_3 = 2$	146	252	1.72
$v_4 = 4$	58	90	1.55
$v_5 = 8$	38	72	1.90
Average of depth ratio			1.43

3.2 Experiment 2

Figure 7 compares the B-scans (cross-sections) perpendicular to the cutting direction for the four most different ablation settings (1 cutting iteration at v_1 , 5 iterations at v_1 , 1 iteration at v_5 , and 5 iterations at v_5). Additionally, we acquired B-scans of the same size at the middle of each line cut showing the bottom of the cut profile along the cutting direction. These B-scans are presented in Figure 7 (e-h) and show that the surface of the cut profile along the cutting direction has some regular unevenness in height (ripples).

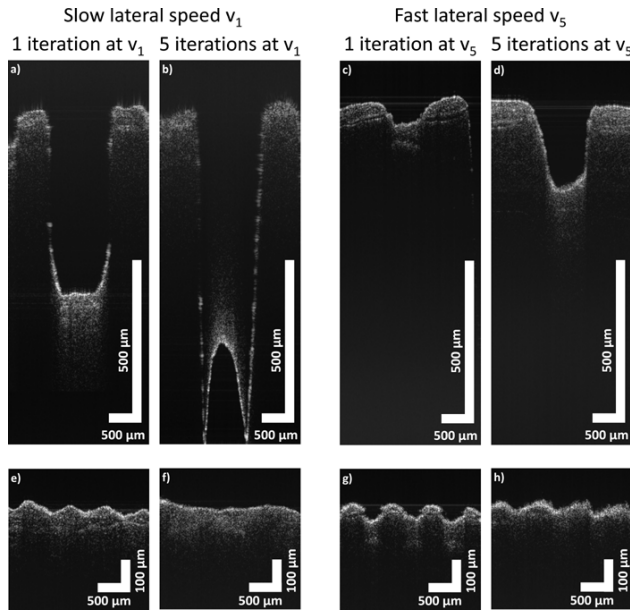


Figure 7: The OCT image shows the comparison of the cut profiles of the four most different ablation settings. Fig. (a-d) show the cut profiles at the middle of each line cut and perpendicular to the lateral cutting direction (YZ-plane). Based on these cross-sections, the cutting depth was determined. Due to the limited depth range of the OCT system, we needed to use both sides of the zero delay to acquire the profile of the deepest cut. As a consequence, the cut profile appears “folded” in the cross-section view (b). However, this has no negative effect on the evaluation of the cutting depth. Fig. (e-h) show the bottom of the ablation crater in the OCT cross-sections at the middle of each line cut along the lateral cutting direction (XY-plane).

In order to obtain comparable measurements for the following evaluation of the cutting depths, we chose the cross-sections (B-scans) perpendicular to the lateral cutting direction containing the deepest ripple.

The crater depths created with the laser system and then measured with OCT are depicted in Figure 8. For each lateral speed, the ablation efficiency changes as the laser is ablating deeper layers (line cut iterations) of the bone.

The ablation area rate is a measure of how efficient the ablation is over time and is given by

$$\text{ablation area rate} = \frac{\text{ablation depth} * \text{lateral speed}}{\text{number of line cut iterations}}. \quad (1)$$

This formula calculates the size of the area that was ablated in 1 second. This area is located in the XY-plane along the lateral cutting direction in the middle of the cut. Figure 9 shows a 3-dimensional contour color map of the ablation area rate for different lateral speeds and up to five line cut iterations.

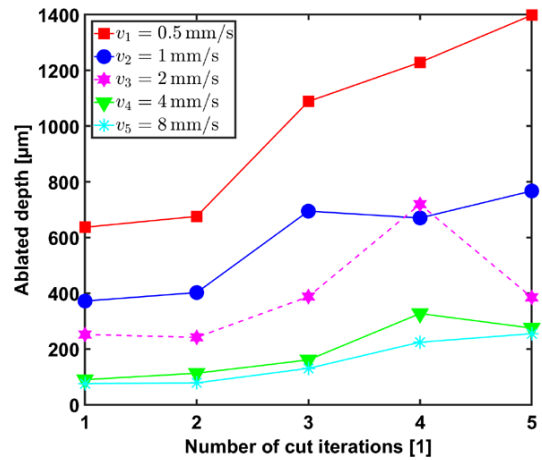


Figure 8: The ablation vs. iteration relation shows the final ablation depths achieved by using different lateral speeds and different number of repetitive line cuts at the same location.

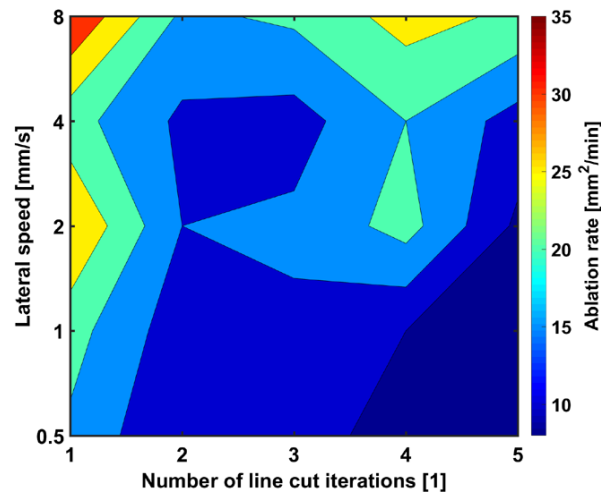


Figure 9: The color-map shows the ablated area in the cross-section perpendicular to the cutting direction over time.

4 Discussion

4.1 Experiment 1

In the first experiment of our study, we aimed to investigate the influence of two different irrigation conditions (shown in Table 1) on the ablation rate of our laser system when ablating bovine femur bone. In a previous study [5], irrigation condition 2 already enabled the best cutting depth (ablation rate) when creating only single holes. In our study on line cutting, we compared two of the irrigation conditions that were used in the previous study among which the best condition was employed again (condition 2). For irrigation condition 1, we achieved the fastest depth increase at the

lateral speed of $v_2 = 1 \frac{\text{mm}}{\text{s}}$, which led to an ablation area rate of $23.28 \frac{\text{mm}^2}{\text{min}}$ (see equation 1). In comparison, for irrigation condition 2, we achieved the fastest depth increase at the lateral speed of $v_5 = 8 \frac{\text{mm}}{\text{s}}$, which corresponds to an ablation area rate of $34.73 \frac{\text{mm}^2}{\text{min}}$. From these results and the ones presented in Table 2, we concluded that irrigation condition 2 provides in total a higher ablation depth than irrigation condition 1. Therefore, we used irrigation condition 2 in experiment 2.

4.2 Experiment 2

The goal of experiment 2 was to investigate the ablation efficiency for deeper cuts and also to observe the quality of the surface after ablation that will result when the laser is moved several times over the same cutting line at different speeds. To limit the number of possible combinations, the best irrigation condition of experiment 1 was employed throughout experiment 2: irrigation condition 2. A maximum of up to 5 repetitions per line cut at the 5 lateral speeds v_1 to v_5 were performed. To ensure a line cut and not several holes separated along the cutting line, we had to limit our lateral speeds to a maximum of $v_5 = 8 \frac{\text{mm}}{\text{s}}$ for the current laser settings (see Figure 7g and 7h). Figure 8 shows, as already demonstrated before for single hole ablation [14], that the ablation depth increases non-linearly as the number of line cuts increases at the same Z-position. This nonlinear behavior is observed for all lateral speeds.

Figure 9 shows that the highest ablation efficiency was obtained with the highest lateral speed and a single line cut; in this case, the achieved ablation area rate was $34.73 \frac{\text{mm}^2}{\text{min}}$ (calculated by equation 1). Furthermore, Figure 9 illustrates that, within the scope of our experiment, it was most efficient to perform a single line cut and to increase the lateral speed until the maximum lateral speed of $8 \frac{\text{mm}}{\text{s}}$. As soon as the maximum lateral speed was reached, we could increase the number of line cut iterations while preserving a high ablation area rate.

Figure 8 shows directly which lateral speed and number of line cut iterations need to be set in order to achieve the desired ablation depth. In the next step, the found pair of values can be compared using Figure 9 to ascertain which combination enables the highest ablation area rate. Thus, these figures can be used as a kind of look-up table for finding the best parameter settings in terms of high ablation rate, which is especially useful in feed-forward control, but also for model-based feedback control.

Besides the efficiency and the ablation depth, there might also be other performance criteria that are impor-

tant for the user such as the smoothness of the surface. Imagine we want to obtain a line cut with a depth around $380 \mu\text{m}$. Figure 8 shows that this cutting depth can be achieved with two different settings; either we perform a single line cut at lateral speed $v_2 = 1 \frac{\text{mm}}{\text{s}}$ or three cutting iterations using scan velocity $v_3 = 2 \frac{\text{mm}}{\text{s}}$. Focusing on the ablation efficiency only (see Figure 9), one single line cut at $v_2 = 1 \frac{\text{mm}}{\text{s}}$ is faster and thereby better setting for this task. Additionally, aiming for a smooth residual cutting surface, Figures 7a and 7g show that using only a single cut iteration leads to a rippled cutting surface for all evaluated lateral speeds v_1 – v_5 . Therefore, more than one cutting iteration is necessary for a smoother surface and this implies that three cutting iterations at the lateral speed $v_3 = 2 \frac{\text{mm}}{\text{s}}$ are the best setting in this case. In short, if a smooth cutting surface is desired, then it is not only the ablation efficiency that matters.

In the depth measurement process, we assumed a flat initial bone surface that was the linear connecting surface between the surrounding non-ablated bone regions. However, the bone surface of every femur is always curved to some extent and has surface irregularities (e. g., little bumps). Thus, if the laser ablation is performed at the valley of a little bump, then the depth of this valley will add up to the cutting depth caused by the laser ablation and in total result in a deeper cut than expected. Moreover, the bone was not well realigned to every new line cut. Thus, the curviness of the bone might cause that the bone surface is not always mounted perpendicularly to the incoming ablation beam. In these cases, it is difficult to define the correct depth offset position of the initial surface, which might cause an inaccuracy in the depth measurement. These reasons could have caused the clearly higher depth (of $719 \mu\text{m}$) measured for the line cut created in four cutting iterations with a lateral speed of $v_3 = 2 \frac{\text{mm}}{\text{s}}$.

4.3 Limitations of the system

To increase the reliability of our results, the experiments should be repeated many times using different bones to enable strict statistical analysis. Additionally, in our study, we controlled the laser ablation in feed-forward mode, laser and irrigation system were not yet synchronized. Measurement outliers as described above might be avoided by using real-time feedback from the OCT system for a closed-loop control of the laser ablation process. However, the implementation of a real-time feedback is a challenging task, since the OCT data processing needs to be speeded-up (usually using the high processing power of

graphics processing units and reducing the region of interest). As an additional constraint for enabling a closed-loop control of the laser ablation system, the data packages and data rates transferred to and in the control loop must allow sufficiently high data rates [19]. Although we are working on the synchronization of the ablation laser, the irrigation system, the OCT system, and the lateral movement of the bone, this synchronization process is not completed yet. Besides the OCT system, additional feedback should be integrated to our system to ensure the proper performance of the complete laser ablation system. This will be particularly important to control the cutting depth online since bones have complex geometric shapes that will require different cutting depths for each spot, e. g., to completely cut through bone.

In a surgery, there are additional parameters that should be taken into consideration. For example, blood is an opaque medium and can absorb the energy of OCT and ablation beams. In order to overcome this issue, bleeding can be removed by an irrigation and suction system. We plan to optimize the timing of the ablation pulse, the irrigation and suction system, as well as the OCT measurement, so that the OCT system measures at the time we expect the least blood content in the cutting area. Moreover, to prevent carbonization of the tissues, the body temperature should be monitored by feedback mechanisms like infrared cameras and the structure of the bone can be monitored by the OCT system.

5 Outlook

In future, we plan to combine the laser ablation beam with the probing beam of the OCT system by a coaxial setup. An important improvement of this combination will be that the location of the bone surface can be measured before any ablation is performed and can be tracked during the ablation process. Measuring the bone surface not only after but also before an ablation will make the estimation of the initial bone surface unnecessary. Thereby, the depth measurement errors arising from curvy and uneven bone surfaces will be eliminated. Additionally, we are currently working on an algorithm for an automatic depth measurement from the cross-sections of the cut profile (as shown in Figure 7). Furthermore, the coordination and synchronization of the different devices involved in laser osteotomy is a challenging task and will be an important part of our future work.

To provide an outlook on our complete system (within the scope of the MIRACLE project) for minimally invasive robot-assisted computer guided laser osteotomy, a control chart is provided that depicts the different system components and also indicates how we plan to close control loops (Figure 10). To find out more about the different system components and their state of development please refer to: [6, 7, 8] for the robotic endoscope tip, [9] for the robotic endoscope, [20] for angle sensors, [21] for shape sensing, and [22, 23, 24] for force sensing of the robotic endoscope,

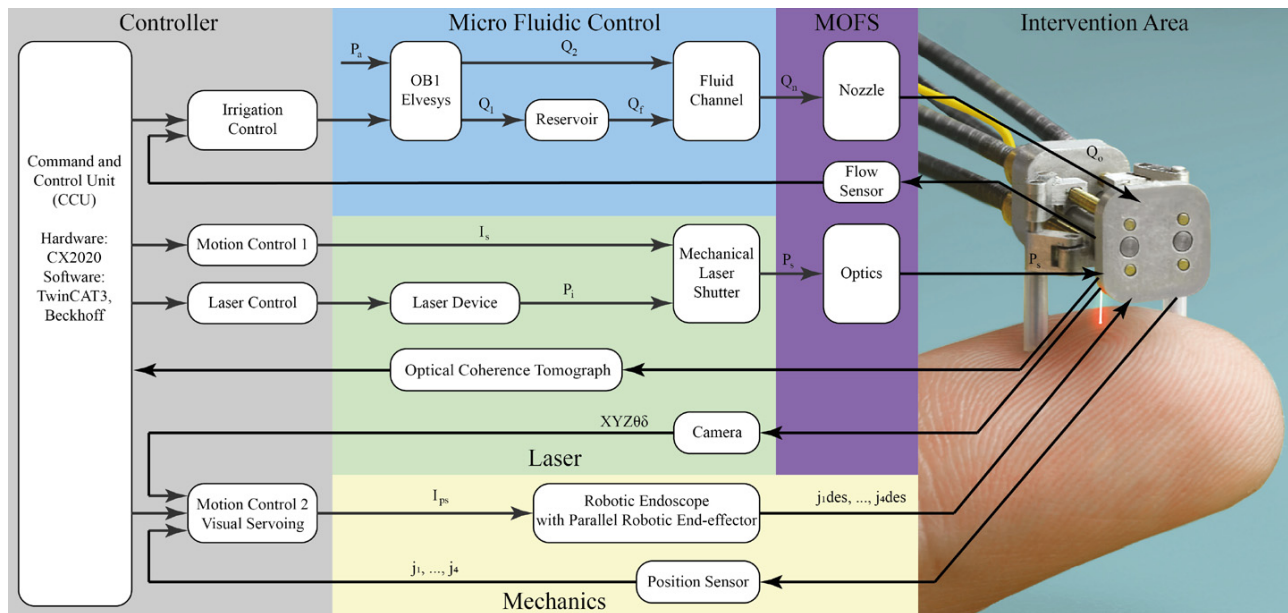


Figure 10: Scheme of the future closed-loop setup for in minimally invasive osteotomy.

[25, 26] laser-induced break down spectroscopy or [27, 28] Mach-Zehnder Interferometry for feedback on tissue types.

6 Conclusion

The current test setup allows a controlled and coordinated testing of different parameters (laser, 3D precision stage, irrigation) for generating continuous cuts in free space experiments. The resulting cutting depth strongly depends on several parameters: the setting of the irrigation system, the lateral speed between the laser and the bone, and the number of line cut iterations at the same location. In experiments, we investigated two irrigation conditions and five different relative speeds between bone and laser (ranging from $0.5 \frac{\text{mm}}{\text{s}}$ to $8 \frac{\text{mm}}{\text{s}}$). We performed additional line cuts on top of the previous one (in total up to five line cuts) at the same Z-position. We could confirm previous work that showed non-linear behaviour of repeated laser cuts at the same spot and expanded this knowledge also to cutting of lines. With the best conditions for the irrigation parameters and constant laser parameters, we obtained the highest ablation area rate of $34.73 \frac{\text{mm}^2}{\text{min}}$ with a lateral speed of $8 \frac{\text{mm}}{\text{s}}$ and a single line cut. Additionally, we obtained a mapping of parameter settings for desired ablation depths, cutting speeds, and repetitions that can be used in feed-forward and closed-loop control of laser ablation. Furthermore, we could give a qualitative impression of what influence these parameters have on the residual surface smoothness.

Acknowledgment: Also, the authors would like to thank Dr. Gabor Kosa, and Dr. Gholamreza Shayeganrad for their support in the planning phase of this paper. In addition, the authors acknowledge Manuela Eugster, Lorin Fasel, and Reinhard Wendler for providing us the robot image used in Figure 10.

Funding: The authors would like to thank the Werner-Siemens foundation for their generous support of this study within the MIRACLE project.

References

1. K.-w. Baek, W. Deibel, D. Marinov, M. Griessen, M. Dard, A. Bruno, H.-F. Zeilhofer, P. Cattin and P. Juergens, "A comparative investigation of bone surface after cutting with mechanical tools and er: Yag laser," *Lasers in surgery and medicine*, vol. 47, no. 5, pp. 426–432, 2015.
2. V. V. Tuchin, "Tissue optics and photonics: Light-tissue interaction ii," *J. of Biomedical Photonics & Eng*, vol. 2, no. 3, 2016.
3. G. Rajitha Gunaratne, R. Khan, D. Fick, B. Robertson, N. Dahotre and C. Ironside, "A review of the physiological and histological effects of laser osteotomy," *Journal of medical engineering & technology*, vol. 41, no. 1, pp. 1–12, 2017.
4. S. R. Visuri, J. T. Walsh and H. A. Wigdor, "Erbium laser ablation of dental hard tissue: effect of water cooling," *Lasers in surgery and medicine*, vol. 18, no. 3, pp. 294–300, 1996.
5. L. M. B. Bernal, G. Shayeganrad, G. Kosa, M. Zelechowski, G. Rauter, N. Friederich, P. C. Cattin and A. Zam, "Performance of er: Yag laser ablation of hard bone under different irrigation water cooling conditions," in *Optical Interactions with Tissue and Cells XXIX*, vol. 10492. International Society for Optics and Photonics, 2018, p. 104920B.
6. M. Eugster, P. Weber, P. Cattin, A. Zam, G. Kosa and G. Rauter, "Positioning and stabilization of a minimally invasive laser osteotome," in *Proceedings of The Hamlyn Symposium on Medical Robotics*. Imperial College London and the Royal Geographical Society, 2017, pp. 21–22.
7. M. Eugster, P. Weber and G. Rauter, "Medical endodevice," Switzerland patenteu European Patent Application EP 17 177 760.0, 6 26, 2017.
8. M. Eugster, E. I. Zoller, L. Fasel, P. C. Cattin, N. F. Friederich, A. Zam and G. Rauter, "Contact force estimation for minimally invasive robot-assisted laser osteotomy in the human knee," in *8th Joint Workshop on New Technologies for Computer/Robot Assisted Surgery, London, 14.–15. September 2018*, Sep. 2018.
9. M. Ahmadi, R. Haji Hassani, G. Kosa, A. Zam, R. Guzman, P. C. Cattin and G. Rauter, "Endocat: An ethercat-based articulated rear view endoscope for single port surgery," in *Biomedical Robotics and Biomechanics (BioRob), 2018 7th IEEE RAS and EMBS International Conference on*. IEEE, 2018, accepted.
10. H. Abbasi, L. Beltrán, G. Rauter, R. Guzman, P. C. Cattin and A. Zam, "Effect of cooling water on ablation in er: Yag laserosteotome of hard bone," in *Third International Conference on Applications of Optics and Photonics*, vol. 10453. International Society for Optics and Photonics, 2017, p. 104531I.
11. L. Beltrán, H. Abbasi, G. Rauter, N. Friederich, P. Cattin and A. Zam, "Effect of laser pulse duration on ablation efficiency of hard bone in microseconds regime," in *Third International Conference on Applications of Optics and Photonics*, vol. 0453. International Society for Optics and Photonics, 2017, p. 104531S.
12. L. Kuscer and J. Diaci, "Measurements of erbium laser-ablation efficiency in hard dental tissues under different water cooling conditions," *Journal of biomedical optics*, vol. 18, no. 10, p. 108002, 2013.
13. A. Fuchs, L. Kahrs and T. Ortmaier, "Optimizing laser ablation parameters and setup for robot-assisted bone cutting and drilling," *Hanover, Germany: Ortmaier Institute of Mechatronic Systems, Leibniz Universität Hannover*, p. 30167, 2014.
14. C.-A. Tulea, J. Caron, N. Geh-lich, A. Lenenbach, R. Noll and P. Loosen, "Laser cutting of bone tissue under bulk water with a pulsed ps-laser at 532 nm," *Journal of biomedical optics*, vol. 20, no. 10, p. 105007, 2015.
15. S. A. Ashforth, M. C. Simpson, O.-e. Bodley and R. Oosterbeek, "Ultrashort pulse laser interactions with cortical bone tissue for

applications in orthopaedic surgery,” in *Frontiers in Ultrafast Optics: Biomedical, Scientific, and Industrial Applications Xv*, vol. 9355. International Society for Optics and Photonics, 2015, p. 935508.

16. A. Fuchs, M. Schultz, A. Krüger, D. Kundrat, J. D. Diaz and T. Ortmaier, “Online measurement and evaluation of the er: Yag laser ablation process using an integrated oct system,” *Biomedical Engineering/Biomedizinische Technik*, vol. 57, no. SI-1 Track-H, pp. 434–437, 2012.
17. O. M. Carrasco-Zevallos, C. Viehland, B. Keller, M. Draelos, A. N. Kuo, C. A. Toth and J. A. Izatt, “Review of intraoperative optical coherence tomography: technology and applications,” *Biomedical optics express*, vol. 8, no. 3, pp. 1607–1637, 2017.
18. M. Wojtkowski, “High-speed optical coherence tomography: basics and applications,” *Applied optics*, vol. 49, no. 16, pp. D30–D61, 2010.
19. Y. Zhang, T. Pfeiffer, M. Weller, W. Wieser, R. Huber, J. Raczkowski, J. Schipper, H. Wörn and T. Klenzner, “Optical coherence tomography guided laser cochleostomy: Towards the accuracy on tens of micrometer scale,” *BioMed research international*, vol. 2014, 2014.
20. L. Iafolla, L. Witthauer, A. Zam, G. Rauter and P. C. Cattin, “Proof of principle of a novel angular sensor concept for tracking systems,” *Sensors and Actuators A: Physical*, 2018. [Online]. Available: <http://www.sciencedirect.com/science/article/pii/S0924424718302462>.
21. S. M. Roodsari, L. Witthauer, L. Iafolla, G. Rauter, A. Zam and P. C. Cattin, “Temperature-compensated fbg-based 3d shape sensor using single-mode fibers,” in *Specialty Optical Fibers*. Optical Society of America, 2018, pp. JTU6C–1.
22. I. Susic, P. Cattin, A. Zam and G. Rauter, “Versatile, force range-adjustable, tri-axial force sensor with integrated micro camera for the tip of endoscopic devices,” in *Proceedings of The Hamlyn Symposium on Medical Robotics*. Imperial College London and the Royal Geographical Society, 2018, pp. 21–22.
23. I. Susic, A. Zam, P. Cattin and G. Rauter, “Enabling minimal invasive palpation in flexible robotic endoscopes,” in *International Workshop on Medical and Service Robots*. Springer, 2018, pp. 64–71.
24. I. Susic and G. Rauter, “Tri-axial force sensor,” Switzerland patent Swiss Patent Application LSP P5572EP00, 6 22, 2018.
25. H. Abbasi, G. Rauter, R. Guzman, P. C. Cattin and A. Zam, “Laser-induced breakdown spectroscopy as a potential tool for autocarbonization detection in laserosteotomy,” *Journal of biomedical optics*, vol. 23, no. 7, p. 071206, 2018.
26. H. Abbasi, G. Rauter, R. Guzman, P. C. Cattin and A. Zam, “Differentiation of femur bone from surrounding soft tissue using laser induced breakdown spectroscopy as a feedback system for smart laserosteotomy,” in *Biophotonics: Photonic Solutions for Better Health Care VI*, vol. 10685. International Society for Optics and Photonics, 2018, p. 1068519.
27. H. N. Kenhagho, G. Rauter, R. Guzman, P. C. Cattin and A. Zam, “Comparison of acoustic shock waves generated by micro and nanosecond lasers for a smart laser surgery system,” in *Advanced Biomedical and Clinical Diagnostic and Surgical Guidance Systems XVI*, vol. 10484. International Society for Optics and Photonics, 2018, p. 104840P.
28. H. N. Kenhagho, G. Rauter, R. Guzman, P. C. Cattin and A. Zam, “Optoacoustic tissue differentiation using a Mach-Zehnder

interferometer: Preliminary results,” in *accepted to be published in IEEE International Ultrasonics Symposium (IUS)*. IEEE Ultrasonics, Ferroelectrics, and Frequency Control Society, 2018.

Bionotes



Lina M. Beltran Bernal
BLOG, Department of Biomedical Engineering, University of Basel, Allschwil, Switzerland
lina.beltran@unibas.ch

Lina Beltrán is a PhD student, her current project is the optimization of the laser system for ablating bone and the fiber system that should be used to achieve endoscopic laser surgery. The optimization also includes the irrigation conditions to improve ablation efficiency without carbonization.



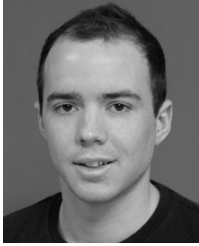
Iris T. Schmidt
BLOG, Department of Biomedical Engineering, University of Basel, Allschwil, Switzerland
iris.schmidt@unibas.ch

Iris Schmidt graduated in Physical Energy and Measurement Technology from Vienna University of Technology in 2016. She is a PhD student in the BLOG, at the DBE, University of Basel. Her main research interest is in developing an optical coherence tomography system for a smart laser surgery system.



Nikola Vulin
Department of Orthopaedics, University of Zurich, Institute for Biomechanics, ETH Zurich, Zurich, Switzerland
nvulin@student.ethz.ch

Nikola Vulin finished his bachelor studies in Mechanical Engineering and continues studying Robotics, System and Control. Nikola is interested in challenging, multidisciplinary topics, where engineering meets biomedical research.



Jonas Widmer
 Department of Orthopaedics, University of Zurich, Institute for Biomechanics, ETH Zurich, Zurich, Switzerland
jonas.widmer@hest.ethz.ch

Jonas Widmer is PhD student with a mechanical engineering background working in the field of spine surgery. Currently working on the development of a fully automatic pipeline to perform biomechanical simulations of spine interventions.



Azhar Zam
 BLOG, Department of Biomedical Engineering, University of Basel, Allschwil, Switzerland
azhar.zam@unibas.ch

Azhar Zam received his PhD in Advanced Optical Technologies from University of Erlangen-Nuremberg, Germany. He is an Assistant Professor at DBE, University of Basel. His main interests are Smart Laser Surgery and Therapy, Optical Coherence Tomography (OCT) and Biomedical Spectroscopy and Imaging.



Jess G. Snedeker
 Department of Orthopaedics, University of Zurich, Institute for Biomechanics, ETH Zurich, Zurich, Switzerland
jess.snedeker@hest.ethz.ch

Jess G. Snedeker was born in the USA. He studied Mechanical and Bioengineering in the USA, and obtained his PhD in Mechanical Engineering from ETH Zurich. In 2006 he became Asst. Prof. and Assoc. Prof. of Orthopedic Biomechanics at ETH Zurich and the University of Zurich, Zurich, Switzerland in 2011.



Georg Rauter
 BIROMED-Lab, Department of Biomedical Engineering, University of Basel, Allschwil and Sensory-Motor Systems Lab, ETH Zurich and Spinal Cord Injury Center, University Hospital Balgrist, Zurich, Switzerland
georg.rauter@unibas.ch

Georg Rauter studied Mechanical Engineering at TU-Graz and Mathematical and Mechanical Modeling at MATMECA, Bordeaux. In 2014 he received his PhD in robotics from ETH Zurich. Since 2016 he heads the BIROMED-Lab as Asst. Prof. for Medical Robotics and Mechatronics at the DBE, University of Basel.



Philippe C. Cattin
 CIAN, Department of Biomedical Engineering, University of Basel, Allschwil, Switzerland
philippe.cattin@unibas.ch

Philippe C. Cattin was born in Switzerland and received his Ph.D. degree 2003 in robotics from ETH Zurich. In 2007 he became an Asst. Professor at the University of Basel and was promoted Assoc. Professor in 2015. Currently he heads the Department of Biomedical Engineering at the University of Basel.